# Density-matrix theory of coherent phonon oscillations in germanium

R. Scholz
*Institut für Theoretische Physik, Rheinisch-Westfälische Technische Hochschule Aachen, Sommerfeldstrasse, D-5100 Aachen, Germany and Scuola Normale Superiore, Piazza dei Cavalieri 7, I-56126 Pisa, Italy*

T. Pfeifer and H. Kurz
*Institut für Halbleitertechnik II, Rheinisch-Westfälische Technische Hochschule Aachen, Sommerfeldstrasse, D-5100 Aachen, Germany*

(Received 17 July 1992; revised manuscript received 4 January 1993)

The generation and detection processes of coherent phonon oscillations in germanium are described within an extended density-matrix model. In the relevant hierarchy of equations of motion for the generation of the phonon oscillation, the anisotropy of the hole distributions related to the anisotropy of the interband dipole matrix elements is identified as the driving force of the coherent vibration. The optical detection of coherent phonons in reflectivity is based on anisotropic band-gap modulations due to the coherent displacements, weighted with the deformation potential of the valence bands.

## I. INTRODUCTION

Coherent phonon oscillations in solids can be excited impulsively by a single femtosecond laser pulse whose duration is shorter than a phonon period. These coherent oscillations are observed in time-resolved optical probing experiments as periodic modulations of reflectivity or transmission. The amplitude and phase of the oscillation are recorded in the time domain by these techniques.

Time-resolved observations of coherent optical phonons have been reported for a large number of solids, e.g., III-V (Ref. 1) and III-VI compounds,[2] group-V elements,[3] and superconductors.[4] Recently, coherent optical phonon oscillations have been observed in germanium.[5]

The first phenomenological explanations of impulsive driving forces are based on the theory of stimulated Raman scattering, but do not include a microscopic model for the derivatives of the dielectric tensor.[6] In the case of III-V semiconductors, the ultrafast charge separation in surface space-charge fields has been identified unambiguously as the driving force.[7,8] For semimetals, a model based on electronically induced displacement of the ion equilibrium coordinates has been proposed.[9]

These considerations cannot be transferred to the case of centrosymmetric semiconductors such as Ge. A theoretical explanation for the optical excitation and optical observation of coherent phonons in this nonpolar material is still missing. The focus of the present paper is to develop a time-dependent theory for the excitation of coherent vibrations in this material, explaining both the observed symmetry and the phase of the oscillation. Each step of the excitation and detection of the phonon oscillation should be described on a microscopic scale.

For these attempts, it is most important to distinguish between a formalism based on transition probabilities, which is generally referred to as Fermi's golden rule, and calculations based on equations of motion for time-dependent observables. The Fermi golden rule treatment requires a separation of time scales between fast oscillations $e^{-i\omega t}$ governed by the energy $\hbar\omega$ of the processes under investigation, and the much longer observation time. In the experiments we want to describe, laser pulses of 50-fs full width at half maximum (FWHM) duration are used to drive and detect oscillations of the optical phonon in Ge with a period of $T=2\pi/\omega=110$ fs. It is obvious that the time scales cannot be separated in this type of experiment.

Methods based on equations of motion for time-dependent quantum correlations can overcome this problem. Two types of formalisms are used: the electronic density matrix, defined as a quantum correlation referring to a single reference time,[10,11] and nonequilibrium Green's-functions techniques describing the propagation of particles between two different microscopic times.[12,13] For the present case, the electronic density-matrix approach is chosen.

In fact, the limits of the applicability of Fermi's golden rule on a femtosecond time scale are not always respected. Calculations based on the electronic density-matrix formalism are able to demonstrate that femtosecond optical pulses drive electronic correlations between degenerate subbands which are not existent in equilibrium but influence transient optical signals.[14,15]

In order to model the coherent-phonon effect, the hierarchy of equations of motion has to be expanded to include fermionic and bosonic observables. Strictly speaking, this extension goes beyond the electronic density matrix. Nevertheless, we call it a density-matrix approach because it is based on equations of motion for quantum correlations referring to a single reference time.

The main result of our investigation is that the anisotropy of the excitation of electron-hole pairs drives the coherent optical-phonon oscillation. Particularly, the anisotropy of nonequilibrium hole distributions in $k$ space launches the coherent modes. Crucial to the selection rules of both the driving force and the detection of the oscillation is the anisotropy of the interband dipole matrix

 

elements, not the anisotropy of the band structure.

In Sec. II, the experimental facts are briefly reviewed. Section III introduces the equations of motion for phononic and electronic quantities in their most general form. In Sec. IV, the relevant iteration path for the generation of the coherent phonons in germanium is identified. This leads to a prediction of the symmetry dependence which meanwhile has been checked experimentally.[5] In Sec. V, the principles for the detection of phonons are presented. The experimental results on the initial phase of the phonon oscillations are discussed in Sec. VI.

## II. EXPERIMENTAL OBSERVATIONS

Irradiation with a single femtosecond laser pulse induces modulations in the reflectivity signal which are monitored by a second attenuated test pulse. Both the excitation and the test pulse have 50-fs duration with 2-eV photon energy. They propagate along the [0,0,1] direction orthogonal to the Ge surface. The excitation pulse is polarized along [1,1,0], while the test field is along [1,0,0]. The reflected pulse is split into components along [1,1,0] and [1,$\bar{1}$,0] and the difference of reflectivities $\Delta R = \Delta R_{\parallel} - \Delta R_{\perp}$ along these polarization directions is recorded. In Fig. 1, the experimentally determined time derivative of this anisotropic reflective response, $\partial(\Delta R)/\partial t$, is shown. A coherent oscillation with a frequency of $\nu = 9.1$ THz is clearly resolved, matching exactly the $\Gamma_{25}$ optical-phonon frequency in germanium.

This detection geometry is analogous to the reflective electro-optic sampling (REOS) technique in polar material,[1] where both the electric field and the phonon displacement contribute to the electro-optic signal. Because the $\chi^{(2)}$ tensor is parity forbidden in nonpolar material, only the deformation-potential interaction remains.

The experimental proof of the theoretically predicted symmetry dependences for the excitation and the detection of the phonon oscillation has been discussed elsewhere in detail.[5] Here we restrict ourselves to reproducing experimental data obtained with the technique analogous to reflective electro-optic sampling, with special emphasis on the initial phase of the coherent oscillation. In time-resolved femtosecond experiments, the zero time delay between pump and test pulses is usually determined through two-photon absorption in GaP crystals. For technical reasons, zero time delay can be determined only with an accuracy of $\pm 10$ fs. Due to these experimental uncertainties, the exact determination of the initial phase of the coherent oscillations is difficult. Therefore we define zero time delay by the moment when the time derivative of the reflectivity change $\partial(\Delta R)/\partial t$ passes through zero. As discussed in detail in Sec. IV, this is a natural reference point for discussing the phonon phase, because memory times and coherence effects influence the dispersive electronic feature in the same way as the phase of phonons.

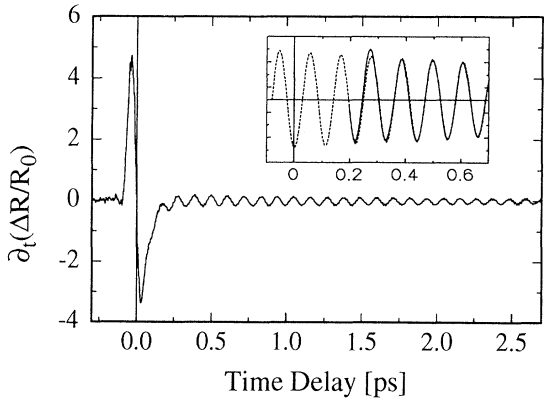


FIG. 1. The time derivative of the anisotropic part of the reflectivity $\Delta R = (\Delta R_{\parallel} - \Delta R_{\perp})$ of the test pulse in arbitrary units. $\Delta R$ means the difference in reflectivity between the $\varphi_t = 45°$ and $-45°$ settings of the test pulse, $\partial/\partial t$ the time derivative. The time axis has been shifted to make the time zero coincide with the dispersive feature near zero delay. The inset shows a fit to the oscillatory part of the data.

The solid line in the inset of Fig. 1 shows the oscillatory part of the reflectivity data differentiated in time between $\Delta t = 200$ and 700 fs. The dashed line is a fit to the measured data, extrapolated back to the time delay $\Delta t = 0$. The experimental data exhibit a clear cosine behavior, indicating a sine behavior of the phonon-induced modulation of the reflectivity itself.

## III. THEORETICAL BACKGROUND: DENSITY-MATRIX FORMALISM

Different representations for the electronic density matrix are used in the literature: a bilocal, a doubled $k$ space, or a mixed $r$-$k$ Wigner representation.[10,11] In the case of spatial invariance, all relevant information is contained in a single $k$-space representation. The equations of motion are derived in a bilocal picture. Since all representations with a complete set of variables are equivalent, Fourier transformations between them are used in the following way in order to obtain the most compact notation in each case. The conduction-band submatrix is denoted by $C_{cc'}$, the valence-band hole submatrix by $D_{vv'}$, and the interband submatrix by $Y_{vc}$.[11]

The commonly used equations of motion for the electronic density matrix contain only the interaction with a light wave. These equations have to be completed by additional terms to include electron-phonon coupling. In this section, we develop a hierarchy of equations of motion including the oscillatory degree of freedom of the optical phonons. A second quantized Hamiltonian in a discrete site representation serves as a starting point.[11,16] By computing this Hamiltonian with two-point fermion operators at the discrete sites, Heisenberg equations of motion for these bilocal quantities can be generated. The equations of motion in continuous spatial variables follow from the equations of motion for the operator-valued quantities at discrete sites by a band-limited interpolation and ensemble averaging.[11,16] Furthermore, equations of motion for phononic quantities $(\hat{a}^{\dagger}_{-\mathbf{q}\lambda}; \hat{a}_{\mathbf{q}\lambda})$ have to be taken into account.

The free phonon Hamiltonian is taken in the standard form. In first order of phonon displacement, the Hamiltonian for electron-phonon coupling can be written as a phonon-assisted hopping between lattice sites $l, j$,

$$\hat{H}_{e,\mathrm{ph}}=\sum_{lj}\left[\sum_{cc'}T^{\mathrm{ph}}_{cjc'l}\hat{C}_{cjc'l}-\sum_{vv'}\hat{T}^{\mathrm{ph}}_{v'lvj}\hat{D}_{vjv'l}\right], \tag{1}$$

where $\hat{T}^{\mathrm{ph}}_{njn'l}$ gives the coupling strength for phonon-assisted transfer between different lattice sites. $\hat{C}_{cjc'l}=\hat{c}^{\dagger}_{cj}\hat{c}_{c'l}$ describes the hopping of an electron from band $c'$ at site $l$ to band $c$ at site $j$, $\hat{D}_{vjv'l}=\hat{d}^{\dagger}_{vj}\hat{d}_{v'l}$ the hole hopping between the valence bands. In order to use the selection rules in the vicinity of symmetry points in the Brillouin zone, it is convenient to transform the operators $\hat{T}^{\mathrm{ph}}_{njn'l}$ into matrix elements between Bloch functions:

$$\hat{T}^{\mathrm{ph}}_{njn'l}=\frac{1}{N}\sum_{\mathbf{q}\lambda}e^{i\mathbf{q}\cdot(\mathbf{R}_j+\mathbf{R}_l)/2}(\hat{a}^{\dagger}_{-\mathbf{q}\lambda}+\hat{a}_{\mathbf{q}\lambda})\times\sum_{\mathbf{k}}e^{i\mathbf{k}\cdot(\mathbf{R}_j-\mathbf{R}_l)}t_{\lambda nn'}(\mathbf{q},\mathbf{k}), \tag{2}$$

where $t_{\lambda nn'}(\mathbf{q},\mathbf{k})$ are matrix elements between lattice periodic parts of Bloch-functions,

$$t_{\lambda nn'}=f_{\lambda n}(\mathbf{q})\delta_{nn'}+\left[\frac{\hbar}{2N\Omega^{5/3}\rho\omega_{\mathbf{q}\lambda}}\right]^{1/2}d_{\lambda nn'}(\mathbf{q},\mathbf{k}), \tag{3}$$

$N$ being the number of unit cells, $\Omega$ the crystal volume, $\rho$ the crystal density, and $\omega_{\mathbf{q}\lambda}$ the phonon frequency. $f_{\lambda n}(\mathbf{q})$ is the matrix element of the long-range Fröhlich interaction, and $d_{\lambda nn'}(\mathbf{q},\mathbf{k})$ the matrix element of the short-range deformation-potential interaction, summed over nonvanishing reciprocal-lattice vectors $\mathbf{Q}$,

$$f_{\lambda n}(\mathbf{q})=-i\sum_{s}\left[\frac{\hbar}{2NM_s\omega_{\mathbf{q}\lambda}}\right]^{1/2}\mathbf{q}\cdot\mathbf{e}_{s\lambda}(\mathbf{q})V_s(\mathbf{q})\langle u_{\mathbf{k}+\mathbf{q}/2,n}(\mathbf{r})|u_{\mathbf{k}-\mathbf{q}/2,n'}(\mathbf{r})\rangle \tag{4}$$

$$d_{\lambda nn'}(\mathbf{q},\mathbf{k})=-\sum_{s}\left[\frac{\rho\Omega}{M_s}\right]^{1/2}\mathbf{e}_{s\lambda}(\mathbf{q})\langle u_{\mathbf{k}+\mathbf{q}/2,n}(\mathbf{r})|\Omega^{1/3}\nabla_r V^d_s(\mathbf{q},\mathbf{r})|u_{\mathbf{k}-\mathbf{q}/2,n'}(\mathbf{r})\rangle \tag{5}$$

$$V^d_s(\mathbf{q},\mathbf{r})=\sum_{\mathbf{Q}\neq 0}V_s(\mathbf{q}+\mathbf{Q})e^{i\mathbf{Q}\cdot\mathbf{r}} \tag{6}$$

where the $u$'s are the lattice periodic parts of the Bloch functions, $M_s$ is the mass of ion $s$, $V_s(\mathbf{q})$ the ionic potential of ion $s$, and $\mathbf{e}_{s\lambda}(\mathbf{q})$ the polarization vector of atom $s$ in mode $\lambda$. The Fröhlich interaction is only present in polar material, while in nonpolar material the contributions of the two ions compensate because of $M_1=M_2$ and $\mathbf{e}_{1\lambda}(\mathbf{q})=-\mathbf{e}_{2\lambda}(\mathbf{q})$. The commutation and band sampling procedure has been described elsewhere,[11,16] and can be worked out by similar algebra. In the following, equations of motion for phononic and electronic quantities are formulated with the full matrix elements $t_{\lambda cc'}(\mathbf{q},\mathbf{k})$ and $t_{\lambda v'v}(\mathbf{q},\mathbf{k})$. They describe both Fröhlich and deformation-potential interactions in polar material, while in Ge only the deformation-potential interaction remains.

### A. Equations of motion for phononic quantities

Two types of phonon observables have to be discussed: occupation numbers $n_{\mathbf{q}\lambda}=\langle\hat{a}^{\dagger}_{\mathbf{q}\lambda}\hat{a}_{\mathbf{q}\lambda}\rangle$ and displacements $\langle(\hat{a}^{\dagger}_{-\mathbf{q}\lambda}+\hat{a}_{\mathbf{q}\lambda})\rangle$. In order to achieve a compact notation, the elements of the electronic density matrix are used here in a Wigner representation. The temporal evolution of phonon occupation numbers is determined by products of operator-valued electronic interband correlations and phonon displacements:

$$\frac{\partial}{\partial t}\langle\hat{a}^{\dagger}_{\mathbf{q}\lambda}\hat{a}_{\mathbf{q}\lambda}\rangle=-\frac{i}{\hbar}\frac{1}{(2\pi)^3}\int d\mathbf{k}\int d\mathbf{R}\,e^{-i\mathbf{q}\cdot\mathbf{R}}\left[\sum_{cc'}t^{*}_{\lambda c'c}(\mathbf{q},\mathbf{k})\langle\hat{a}^{\dagger}_{\mathbf{q}\lambda}\hat{C}_{cc'}(\mathbf{R},\mathbf{k})\rangle-\sum_{vv'}t^{*}_{\lambda vv'}(\mathbf{q},\mathbf{k})\langle\hat{a}^{\dagger}_{\mathbf{q}\lambda}\hat{D}_{vv'}(\mathbf{R},\mathbf{k})\rangle\right]$$
$$+\frac{i}{\hbar}\frac{1}{(2\pi)^3}\int d\mathbf{k}\int d\mathbf{R}\,e^{i\mathbf{q}\cdot\mathbf{R}}\left[\sum_{cc'}t_{\lambda cc'}(\mathbf{q},\mathbf{k})\langle\hat{a}_{\mathbf{q}\lambda}\hat{C}_{cc'}(\mathbf{R},\mathbf{k})\rangle-\sum_{vv'}t_{\lambda v'v}(\mathbf{q},\mathbf{k})\langle\hat{a}_{\mathbf{q}\lambda}\hat{D}_{vv'}(\mathbf{R},\mathbf{k})\rangle\right]. \tag{7}$$

An analysis of the averages and fluctuations of the phonon-assisted quantities on the right-hand side would lead to a time-dependent damping theory without the long-time limit inherent in usual scattering terms in the frame of Fermi's golden rule (non-Markovian scattering).[17] The full information of the six-dimensional space of variables for the electronic correlations is important, because the neglect of the midpoint coordinate $\mathbf{R}$ would lead to a change in the $\mathbf{q}=\mathbf{0}$ phonon occupation number only. We will not stress this point further, but concentrate on the time-dependent phonon displacements. It is convenient to introduce differential equations of second order, giving the usual differential operator of a harmonic oscillator:

$$\left[\frac{\partial^2}{\partial t^2}+\omega^2_{\mathbf{q}\lambda}\right]\langle(\hat{a}^{\dagger}_{-\mathbf{q}\lambda}+\hat{a}_{\mathbf{q}\lambda})\rangle=-\frac{2\omega_{\mathbf{q}\lambda}}{\hbar}\frac{1}{(2\pi)^3}\int d\mathbf{k}\int d\mathbf{R}\,e^{-i\mathbf{q}\cdot\mathbf{R}}\left[\sum_{c,c'}t^{*}_{\lambda c'c}(\mathbf{q},\mathbf{k})C_{cc'}(\mathbf{R},\mathbf{k})-\sum_{v,v'}t^{*}_{\lambda vv'}(\mathbf{q},\mathbf{k})D_{vv'}(\mathbf{R},\mathbf{k})\right]. \tag{8}$$

In polar materials, the Fröhlich part of the source terms is constituted by the electromagnetic coupling of monopolar charge densities to the lattice polarization. Coherent phonon oscillations can then be driven by the ultrafast separation

of electrons and holes in the region of band bending and boundary fields near the surface,[7,8] which constitutes the dominating driving mechanism. Corrections due to the deformation potential have not yet been observed, because their contribution to the signal amplitude is of the order of only 1%.

Since the Fröhlich coupling is absent in germanium, the deformation-potential interaction remains the only driving force for coherent phonons,[5] as will be discussed in Sec. IV in more detail.

### B. Modifications of the equations of motion for the electronic density matrix

Optical experiments performed with a photon energy of 2 eV, high above the gap energy of 0.8 eV in germanium, mainly measure interband quantities between valence and conduction bands. Therefore it is sufficient to consider the modifications of the interband equation of motion by the electron-phonon interaction. The additional terms in the equation of motion for the interband density $Y_{vc}$ are the following:

$$\frac{\partial}{\partial t}Y_{vc}(\mathbf{r}_1,\mathbf{r}_2)+i\Omega_{vc}Y_{vc}(\mathbf{r}_1,\mathbf{r}_2)=\frac{i}{\hbar}\mathbf{E}(\mathbf{R})\mathbf{M}_{cv}(\mathbf{r})+\frac{i}{\hbar}\sum_{\mathbf{q}\lambda}\sum_{v'}e^{i\mathbf{q}\cdot\mathbf{r}_1}t_{\lambda v'v}(\mathbf{q},+i\nabla_1-\mathbf{q}/2)\langle(\hat{a}^{\dagger}_{-\mathbf{q}\lambda}+\hat{a}_{\mathbf{q}\lambda})\hat{Y}_{v'c}(\mathbf{r}_1,\mathbf{r}_2)\rangle$$

$$-\frac{i}{\hbar}\sum_{\mathbf{q}\lambda}\sum_{c'}e^{i\mathbf{q}\cdot\mathbf{r}_2}t_{\lambda cc'}(\mathbf{q},-i\nabla_2+\mathbf{q}/2)\langle(\hat{a}^{\dagger}_{-\mathbf{q}\lambda}+\hat{a}_{\mathbf{q}\lambda})\hat{Y}_{vc'}(\mathbf{r}_1,\mathbf{r}_2)\rangle\ , \tag{9}$$

where $\Omega_{vc}$ is the gap operator in the bilocal representation and $\mathbf{M}_{cv}(\mathbf{r})$ is the interband dipole-matrix element in the notation of Refs. 11, 14, and 16. Saturation terms due to Pauli blocking[14,16] are not written explicitly. When the phonon displacement $\langle(\hat{a}^{\dagger}_{-\mathbf{q}\lambda}+\hat{a}_{\mathbf{q}\lambda})\rangle$ is a nonvanishing quantity, the ensemble averages $\langle(\hat{a}^{\dagger}_{-\mathbf{q}\lambda}+\hat{a}_{\mathbf{q}\lambda})\hat{Y}_{v'c}(\mathbf{r}_1,\mathbf{r}_2)\rangle$ in Eq. (9) can be replaced by the product of averages. According to Eq. (8), this is only possible if the displacement $\langle(\hat{a}^{\dagger}_{\mathbf{q}\lambda}+\hat{a}_{\mathbf{q}\lambda})\rangle$ is driven resonantly by electron- and hole-density matrices.

## IV. DRIVING OF COHERENT PHONON OSCILLATIONS IN GERMANIUM

In the coherent phonon experiments in Ge, the electron-hole pairs are generated with an excitation pulse of 50-fs duration and a photon energy of 2 eV. The electric field $\mathbf{E}_e(\mathbf{R},t)$ of this pulse can be written as

$$\mathbf{E}_e(\mathbf{R},t)=[\mathbf{e}_e e^{i\mathbf{k}_e\cdot\mathbf{R}-i\omega_e t}+\text{c.c.}]F_e(t)\ , \tag{10}$$

where $\mathbf{e}_e=[\cos\varphi_e,\sin\varphi_e,0]$ is the polarization vector, $\mathbf{k}_e\|[0,0,1]$ the direction of propagation normal to the surface, $\omega_e$ the photon frequency, and $F_e(t)$ the pulse envelope.

Because of the selection rules related to the interband dipole-matrix elements,[10,14] the carriers are excited in anisotropic $k$-space distributions. It has been shown recently that "coherent" peaks in time-resolved transmission experiments can be explained by the simple assumption that the anisotropic nonthermal parts of the carrier distributions will relax to hot thermalized distributions within characteristic times $\tau_{ee}$ and $\tau_{hh}$ for electrons and holes, respectively.[14,16] Both times are determined by all scattering events involved and are of the order of 10–20 fs. Cooling of the hot thermalized distributions toward lattice temperature takes place on a much slower time scale.[16,18] The total particle distributions are composed of coherent and thermalized parts, e.g., $D_{vv'}=D^{\text{coh}}_{vv'}+D^{\text{th}}_{vv'}$. For intersubband correlations with $v\neq v'$, the thermalized parts vanish. The equation of motion of the coherent anisotropic distributions $D^{\text{coh}}_{vv'}$ can be described explicitly by[14,16]

$$\frac{\partial}{\partial t}D^{\text{coh}}_{vv'}(\mathbf{R},-\mathbf{k})+\frac{1}{\tau_{\text{hh}}}D^{\text{coh}}_{vv'}(\mathbf{R},-\mathbf{k})$$

$$=-\frac{i}{\hbar}\mathbf{E}_e(\mathbf{R})\left[\sum_c\mathbf{M}^*_{cv}(\mathbf{k})Y_{v'c}(\mathbf{R},\mathbf{k})-\sum_c\mathbf{M}_{cv'}(\mathbf{k})Y^*_{vc}(\mathbf{R},\mathbf{k})\right]\ . \tag{11}$$

The resulting coherent anisotropic hole matrix $D$ of second order in the exciting field reads

$$D^{\text{coh}(2)}_{vv'}(\mathbf{R},-\mathbf{k})=\frac{1}{\hbar^2}\sum_c[\mathbf{e}^*_e\mathbf{M}^*_{cv}(\mathbf{k})][\mathbf{e}_e\mathbf{M}_{cv'}(\mathbf{k})]G_{vv'}[e^{i\omega_e t}F_e(t)G_{v'c}\{e^{-i\omega_e t}F_e(t)\}]$$

$$+\frac{1}{\hbar^2}\sum_c[\mathbf{e}_e\mathbf{M}_{cv'}(\mathbf{k})][\mathbf{e}^*_e\mathbf{M}^*_{cv}(\mathbf{k})]G_{vv'}(e^{-i\omega_e t}F_e(t)[G_{vc}\{e^{-i\omega_e t}F_e(t)\}]^*) \tag{12}$$

with the Green's functions $G_{vv'}$ of the valence-band equation:

$$G_{vv'}\{f(t)\}=\int_{-\infty}^{0}d\tau\,e^{\tau/\tau_{\text{hh}}}f(t+\tau) \tag{13}$$

and $G_{vc}$ of the interband equation:

$$G_{vc}\{e^{-i\omega_e t}F_e(t)\}=f_{\text{coul}}(\hbar\omega_{gvc}(\mathbf{k}))e^{-i\omega_e t}\times\int_{-\infty}^{0}d\tau\,e^{\gamma\tau}e^{i[\omega_{gvc}(\mathbf{k})-\omega_e]\tau}F_e(t+\tau)\ , \tag{14}$$

where $f_{\text{coul}}$ is the Coulomb enhancement factor.[14,16,18] The distributions $D^{\text{coh}}_{vv'}$ are called "coherent" because they

are determined by the resonance condition and symmetry of the excitation. Two types of anisotropies are involved: The anisotropy of the band gap $\omega_{gvc}(\mathbf{k})$ and the anisotropy of the interband dipole matrix element $M_{cv'}(\mathbf{k})$ and $M^*_{cv}(\mathbf{k})$.

An interpolation of recent low-temperature band-structure calculations[19] to room-temperature measurements of the $E_0$ and $E_1$ gaps[20] indicates that resonant excitation with 2-eV photons occurs on an extremely anisotropic $k$ shell: for $\mathbf{k}$ along $\Delta$, e.g., $\mathbf{k}\|[1,0,0]$, the heavy-hole resonance occurs at $|\mathbf{k}|=0.13(2\pi/a)$, while for $k$ along $\Lambda$, e.g., $\mathbf{k}\|[1,1,1]$, the resonance is located at $|\mathbf{k}|=0.44(2\pi/a)$, which is near the midpoint between $\Gamma$ and $L$. The band structure implies that the $E_1$ gap is a $M_1$ critical point at or very near the $L$ point.[19] This resonance is considerably broadened at room temperature: $\hbar\gamma=58$ meV, i.e., $T_2=11$ fs.[20] This large broadening for transitions with $k$ along $\Lambda$ indicates that a large portion of the $\Lambda$ region is resonantly coupled by 2-eV photons, even if the $E_1$ gap is at 2.11 eV.[20]

For transitions from the light-hole band, the anisotropy is less pronounced: $|\mathbf{k}|=0.12(2\pi/a)$ for $\mathbf{k}$ along $\Delta$ and $|\mathbf{k}|=0.22(2\pi/a)$ for $\mathbf{k}$ along $\Lambda$.[19] The smaller $\mathbf{k}$ reduces the optical density of states, and the broadening of the $(E_1+\Delta_1)$ gap of 74 meV (Ref. 20) should be reduced in the vicinity of $\Gamma$. For the split-off transition, the anisotropy is even weaker, and the optical density of states lower because of the smaller $k$ vectors involved.

Recent photon echo measurements in GaAs demonstrate that the dephasing time $T_2$ of the interband transitions is strongly density dependent.[21] Interpolating these results to our excitation density of $n=3\times10^{19}$ cm$^{-3}$ yields a dephasing time of $T_2=8$ fs. This value can be regarded as an upper limit for Ge, because already at low density, the dephasing times at 2 eV are considerably shorter than in GaAs.[20,21]

The investigation of the coupling symmetries has to be based on the star of a given wave vector $\mathbf{k}$, because each star can be used as a representation of the point group.[22] The star of $\mathbf{k}$ is the set of distinct wave vectors $\mathbf{k}'=g\mathbf{k}$ found when applying the group elements $g$ of the point group to $\mathbf{k}$. The gap energy is anisotropic in $k$ space, but each star of a fixed $\mathbf{k}$ has the same gap for all wave vectors of the star. A second anisotropy arises because of the exciting electric field, $[\mathbf{e}_e\mathbf{M}_{cv'}(\mathbf{k})][\mathbf{e}_e^*\mathbf{M}^*_{cv}(\mathbf{k})]$. This second type of anisotropy relaxes on a typical time scale of $\tau_{\rm hh}$, compare Eq. (11). From model calculations for GaAs at much lower density, $n=1.0\times10^{18}$ cm$^{-3}$, an upper limit of $\tau_{\rm hh}$ in the present case is derived: $\tau_{\rm hh}<13$ fs.[14–16] Within this time, internal thermalization of holes occurs, still preserving anisotropies of the band structure, but with equal populations for all $\mathbf{k}$ of the same star.

Under the conditions pertinent to the excitation of Ge, Eq. (8) can be transformed into

$$\left[\frac{\partial^2}{\partial t^2}+2\Gamma_{\rm ph}\frac{\partial}{\partial t}+\omega^2_{\mathbf{q}\lambda}\right]\langle(\hat{a}^\dagger_{-\mathbf{q}\lambda}+\hat{a}_{\mathbf{q}\lambda})\rangle = \frac{2\omega_{\rm TO}}{\hbar}\frac{1}{(2\pi)^3}\int d\mathbf{k}\sum_{vv'} d^*_{\lambda vv'}(\mathbf{q},\mathbf{k})D^{\rm coh(2)}_{vv'}(\mathbf{q},\mathbf{k})\ . \quad (15)$$

$\omega_{\rm TO}$ is the optical phonon frequency at $\mathbf{q}=0$, where transverse and longitudinal phonons are degenerate, and $\Gamma_{\rm ph}$ is a phenomenological dephasing rate. $D^{\rm coh}_{vv'}(\mathbf{q},\mathbf{k})$ is the Fourier transform of the Wigner distribution, $D^{\rm coh}_{vv'}(\mathbf{R},\mathbf{k})$. $\mathbf{q}$ describes the spatial inhomogeneity of the hole distribution, while $\mathbf{k}$ gives the momentum distribution. Because the excitation creates a disklike hole distribution in real space, the wave vectors $\mathbf{q}$ exhibit a cigar-like distribution. This anisotropy drives longitudinal phonons with $\mathbf{q}\simeq q\mathbf{e}_z$. The hole wave vector $\mathbf{q}$ is of the order of the inverse penetration depth of the light wave, which is very small compared to the electronic $k$ vectors at resonant excitation with 2-eV photons. Therefore the inequality $q\ll k$ holds for all transitions involved, and the phonon wave vector $q$ can be neglected in the deformation-potential matrix element. The selection rule for the coupling of the holes to the phonon displacement consists of three parts: two dipole-matrix elements $\mathbf{M}$ and $\mathbf{M}^*$ according to Eq. (12), and one matrix element of the phonon deformation potential, $d^*_{\lambda vv'}(\mathbf{0},\mathbf{k})$, compare Eq. (15):

$$\sum_c [\mathbf{e}_e\mathbf{M}_{cv'}(\mathbf{k})][\mathbf{e}_e^*\mathbf{M}^*_{cv}(\mathbf{k})]d^*_{\lambda vv'}(\mathbf{0},\mathbf{k}) = \sum_{i,j}\mathbf{e}_{e,i}\mathbf{e}^*_{e,j}\{[\mathbf{M}_{cv',i}(\mathbf{k})\mathbf{M}^*_{cv,j}(\mathbf{k})]d^*_{\lambda vv'}(\mathbf{0},\mathbf{k})\} \equiv \sum_{i,j}\mathbf{e}_{e,i}\mathbf{e}^*_{e,j}A_{\lambda v'v,ij}(\mathbf{k})\ . \quad (16)$$

The optical-phonon modes transform like $yz$, $zx$, and $xy$,[23,24] while the transition dipole-matrix elements are polar vectors, leading to a total transformation behavior of a fourth rank tensor. Our excitation geometry requires that the electric field of the exciting light pulse be in the $xy$ plane, i.e., $i,j\in\{x,y\}$. After averaging $A_{\lambda v'v,ij}(\mathbf{k})$ over the star of a given wave vector $\mathbf{k}$, the well-known restrictions of tensor elements in cubic crystals apply,[25] leading to the selection rule that only the phonon mode $\lambda=z$ transforming like $xy$ contributes:

$$\sum_{\mathbf{k}'\in\{\rm stark\}}A_{zv'v}(\mathbf{k}')\propto\begin{bmatrix}0&1&0\\1&0&0\\0&0&0\end{bmatrix}\ . \quad (17)$$

It is important to consider the whole star of wave vectors at once, because the symmetry restrictions do not apply to each wave vector separately, but only to the smallest set of wave vectors being a representation of the point group.

The thermalized holes cannot exert a driving force, because they have equal occupation numbers for all wave vectors belonging to the same star. This leads to an averaging of phononic tensor quantities transforming like $yz$, $xz$, and $xy$ over each star. Because of the restrictions of the cubic crystal symmetry, the sum over the star has to vanish.[25] The coherent parts of the electron distributions can in principle act as a driving force, but as their deformation potential vanishes at $\Gamma$, their contributions at finite wave vector are much smaller than those of the holes.

The total selection rule of the driving force corre-

sponds to the Raman tensor of the optical phonons. Unfortunately, this Raman tensor is usually defined, including the in and out resonances[24] which do not change the selection rule. For time-resolved optics, it is more appropriate to treat the resonance conditions in the form of time-dependent functions, as in Eqs. (12)–(15), instead of resonance denominators adapted to stationary processes.[24]

For small $\mathbf{k}$, the matrix elements can be calculated for any arbitrary orientation of $\mathbf{k}$ with wave functions derived from the Kane model.[26] These approximate wave functions are widely used to explore anisotropies encountered during polarized optical excitation, $[\mathbf{e}_e\mathbf{M}_{cv'}(\mathbf{k})][\mathbf{e}_e^*\mathbf{M}_{cv}^*(\mathbf{k})]$.[10,14,26,27] A calculation of $A_{zv'v}(\mathbf{k})$ within this model allows an estimate of the coupling strength near $\Gamma$.[16]

The anisotropy of the hole distribution arising from the dipole-matrix elements is crucial for generating coherent phonon oscillations: In the case of thermalized hole distribution, the deformation potentials are averaged to zero, as mentioned above. The observation of coherent phonons in Ge is therefore a direct proof of the existence of this type of anisotropy during the optical excitation. If the linearly polarized excitation pulse propagates along [0,0,1], coherent oscillations are driven with an amplitude proportion to $\sin(2\varphi_e)$, compare Eqs. (16) and (17). This excitation symmetry is confirmed in experiments.[5] The selection rule for the driving force due to the anisotropic part of the hole distributions can be interpreted as an anisotropic weakening of the bonds between adjacent germanium atoms. Each Ge atom has four next neighbors in tetrahedral configuration, bridged by binding valence orbitals. The excitation of electron-hole pairs weakens the strength of bonding. As long as the hole distribution is anisotropically distributed over the star of a given $\mathbf{k}$, the weakening is distributed anisotropically over the four bonds. Two of the bonds form an angle of 35° with the [1,1,0] direction while they are orthogonal on the $[1,-1,0]$ direction. For the other two bonds, the reverse is true: They form an angle of 35° with the $[1,-1,0]$ direction and are orthogonal on [1,1,0]. When the polarization of the excitation pulse is along [1,1,0], i.e., $\varphi_e=45°$, the holes are excited mainly from one of these groups of bonds. If the polarization is turned from [1,1,0] to $[1,-1,0]$, i.e., from $\varphi_e=45°$ to $\varphi_e=-45°$, the roles of the bonds interchange. This results in a phase change of 180° in the phonon oscillation, or in a change of sign, according to $\sin(2\varphi_e)=1$ for $\varphi_e=45°$ and $\sin(2\varphi_e)=-1$ for $\varphi_e=-45°$.

## V. DETECTION OF THE OSCILLATION BY THE TEST PULSE

The phonon oscillation is detected via an anisotropic modulation of the reflectivity of the test pulse. As the phonon displacement is a nonvanishing quantity, the phonon-assisted source terms in the basic equation (9) can be replaced by the products of electronic and phononic quantities. The interband polarization $\mathbf{P}$ is related to the interband matrix $Y$ as follows:[11,16]

$$\mathbf{P}(\mathbf{R},t)=\sum_{cv}\frac{1}{(2\pi)^3}\int d\mathbf{k}[\mathbf{M}_{cv}^*(\mathbf{k})Y_{vc}(\mathbf{R},\mathbf{k},t)+\mathbf{M}_{cv}(\mathbf{k})Y_{vc}^*(\mathbf{R},\mathbf{k},t)]\ . \tag{18}$$

Considering the selection rules to leading order in the wave vector, the mixing of the conduction bands by the phonon displacement is forbidden by symmetry. The relevant equation of motion for $Y$ is therefore

$$\frac{\partial}{\partial t}Y_{vc}(\mathbf{r}_1,\mathbf{r}_2)+i\Omega_{vc}Y_{vc}(\mathbf{r}_1,\mathbf{r}_2)=\frac{i}{\hbar}\mathbf{E}(\mathbf{R})\mathbf{M}_{cv}(\mathbf{r})+\frac{i}{\hbar}\sum_{\mathbf{q}\lambda}\sum_{v'}e^{i\mathbf{q}\cdot\mathbf{r}_1}d_{\lambda v'v}(\mathbf{0},\mathbf{k})\times\langle(\hat{a}^\dagger_{-\mathbf{q}\lambda}+\hat{a}_{\mathbf{q}\lambda})\rangle\times\hat{Y}_{v'c}(\mathbf{r}_1,\mathbf{r}_2)\ . \tag{19}$$

Saturation terms with $C$ and $D$ have been neglected; their features in femtosecond experiments have been discussed in detail elsewhere.[14,16] In analogy to the excitation field, the electric field of the test pulse is parametrized by

$$\mathbf{E}_t(\mathbf{R},t)=[\mathbf{e}_te^{i\mathbf{k}_t\cdot\mathbf{R}-i\omega_t t}+\text{c.c.}]F_t(t)\ , \tag{20}$$

where $\mathbf{e}_t=[\cos\varphi_t,\sin\varphi_t,0]$ is the polarization of the test field, and $\mathbf{k}_t\|[0,0,1]$ is the direction of propagation. In first order, an interband density $Y_{vc}^{(1)}$ arises according to Eq. (19). Together with the phonon displacement $\langle(\hat{a}^\dagger_{-\mathbf{q}\lambda}+\hat{a}_{\mathbf{q}\lambda})\rangle$, this interband density gives rise to the second term in the source of Eq. (19), leading to an interband matrix $Y_{vc}^{(2)}$ which is a linear function of the phonon displacement $\langle(\hat{a}^\dagger_{-\mathbf{q}\lambda}+\hat{a}_{\mathbf{q}\lambda})\rangle$ and of the first-order interband matrix $Y_{v'c}^{(1)}$. The diagonal contributions in the valence-band indices $v=v'$ dominate because of resonance arguments. The effect of the phonon oscillation therefore can be understood as an anisotropic modulation of the valence bands in $k$ space, leading to an anisotropic modulation of the band gaps.

As discussed above, the excitation field drives only the phonon mode orthogonal to the surface, $\lambda=z,\mathbf{q}\|\mathbf{e}_z$. The selection rule of the phonon-assisted polarization driven by the test field again consists of three parts: the optical dipole-matrix element $\mathbf{M}^*$ relating the interband density $Y_{vc}(\mathbf{R},\mathbf{r})$ to the polarization $\mathbf{P}^{(2)}$ according to Eq. (18); the deformation potential $d_{\lambda v'v}(\mathbf{0},\mathbf{k})$; and the dipole matrix element $\mathbf{M}$ hidden in the linear interband density $Y_{v'c}(\mathbf{R},\mathbf{r})$ in the second source term of (19). Therefore the overall selection rule is similar to the excitation of the coherent oscillation, compare Eqs. (16) and (17). The anisotropic part of the polarization, $\mathbf{P}^{(2)}$, is then proportional to

$$\mathbf{P}^{(2)} \propto \begin{bmatrix} 0 & 1 & 0 \\ 1 & 0 & 0 \\ 0 & 0 & 0 \end{bmatrix} \mathbf{e}_t = \sin(2\varphi_t) \begin{bmatrix} \cos\varphi_t \\ \sin\varphi_t \\ 0 \end{bmatrix} + \cos(2\varphi_t) \begin{bmatrix} -\sin\varphi_t \\ \cos\varphi_t \\ 0 \end{bmatrix} . \tag{21}$$

The first term leads to an additional polarization along $\mathbf{e}_t$, the second to a polarization orthogonal to $\mathbf{e}_t$. Unless unusual experimental techniques are employed, only contributions along $\mathbf{e}_t$ can be observed. The reason for this is that the second term leads only to a slight change in the direction of polarization of the reflected test pulse, while the reflected intensity is only affected in second order. With the present experimental setup, a sufficient suppression of the reflected signal with polarization along $\mathbf{e}_t$ is not possible. If the reflected beam is not passed through a polarizer, the reflected signal is proportional to $\sin(2\varphi_t)$, since the second-order contribution coming from the second term in Eq. (21) remains too small to be observed. Therefore the overall selection rule for the test field is the same as for driving the oscillation by the excitation pulse.

## VI. THE INITIAL PHASE OF THE COHERENT OSCILLATIONS

The dispersive feature of $\partial(\Delta R)/\partial t = \partial(\Delta R_{\parallel} - \Delta R_{\perp})/\partial t$ in Fig. 1 around time delay $\Delta t = 0$ arises from coherent electronic contributions, affecting especially the reflected intensity $\Delta R_{\parallel}$ when the polarization of the excitation and test pulses are parallel. The coherent coupling can be interpreted as Pauli blocking of the interband transition by anisotropic unrelaxed carrier contributions.[14,16] The buildup of the anisotropic electron and hole distributions peaks slightly after the maximum of the excitation pulse. From a theoretical point of view, an additional time shift in the probe signal is expected by the finite-phase relaxation time $T_2$, because the anisotropic saturation terms have to be inserted into the interband source.[14,16] The maximum of the anisotropic electronic part of the reflectivity change, $\Delta R = (\Delta R_{\parallel} - \Delta R_{\perp})$, is expected to occur at a certain positive time delay $\Delta t$ after the actual time delay $\Delta t = 0$, defined by the temporal coincidence of the intensity maxima of excitation and test pulse.[14,15]

Setting the time delay zero of $\partial(\Delta R)/\partial t$ in Fig. 1 to the moment of passing through the 0 line means that we define the time zero of the plot as the moment at which the maximum of the anisotropic reflectivity is induced. The theoretical model, presented above, leads to the conclusion that the coherent anisotropic hole distributions act as the driving force of the coherent phonons in Ge. The temporal evolution of the driving force is determined by the buildup and relaxation of the anisotropic hole distributions. The detection of both, the reflectivity maximum due to nonthermalized carriers as well as the phonon-induced reflectivity modulations implies additional temporal shifts due to the finite-phase relaxation time $T_2$. Both the temporal delay due to the buildup of anisotropic carrier distributions as well as the temporal delay due to the $T_2$-damped interband response are canceled, because they are operative in the anisotropic Pauli blocking in the same way as in the phonon-induced part of the reflectivity. As a consequence, the phonon-induced reflectivity modulation should exhibit a sine behavior with respect to our reference time. Because the total time shift of both kinds of reflectivity signatures, the oscillating and the nonoscillating part, are of the order of a quarter of an oscillation period,[15] it is important to use the shifted time axis of Fig. 1, where the influence of coherence and relaxation times cancels.

In the inset of Fig. 1, the oscillatory fit to the data taken at delays $\Delta t > 200$ fs is extrapolated back to zero time delay as defined above. It turns out that the oscillatory part of the time derivative of the reflectivity can be described by a damped cosine function in time, phase shifted by less than 2 fs.[5] This means that the oscillatory part of the reflectivity itself can be described by a damped sine function, which is a direct proof of our theoretical considerations.

A crucial experiment for the checking of our arguments would be the exchange of excitation and test pulse.[9] This would provide the possibility of measuring the joint effects of the lifetime $\tau_{hh}$ of nonthermal holes and the phase relaxation time $T_2$. The analysis of electronic anisotropic reflectivity contributions and the phase of phonon-induced modulations would yield upper and lower limits for these microscopic relaxation times.

## VII. CONCLUSIONS

In this paper, the excitation and detection of coherent phonons in germanium are described within an extended density-matrix model, going beyond the possibilities of a Fermi golden rule treatment. The usual semiconductor Bloch equations are completed by additional terms due to electron-phonon coupling and by equations of motion for phononic quantities.

The selection rules for the generation and detection of the optical-phonon oscillations are explained as the joint effect of two dipole matrix elements and the deformation potential of the phonon. The driving force of the oscillation is related to the formation of anisotropic hole distributions during the excitation process, exhibiting the symmetry of the interband dipole-matrix elements. The detection involves anisotropic band-gap modulations by the optical phonon displacement.

The initial phase of the coherent optical phonon is derived as a sine with respect to the maxima of the anisotropic contributions to the reflectivity, as confirmed by experimental results.

## ACKNOWLEDGMENTS

We would like to thank A. Stahl, W. Kütt, and H. J. Bakker for intense and useful discussions, and A. Esser and G. Maidorn for providing experimental data. This work has been supported by the Alfried Krupp Foundation and by the Deutsche Forschungsgemeinschaft (DFG).

[1]G. C. Cho, W. Kütt, and H. Kurz, Phys. Rev. Lett. **65**, 764 (1990).

[2]K. Seibert, H. Heesel, W. Albrecht, J. Geurts, K. Allakhverdiev, and H. Kurz, in *The 20th International Conference on the Physics of Semiconductors 3,* edited by E. M. Anastassakis and J. D. Joannopoulos (World Scientific, London, 1990).

[3]T. K. Cheng, S. Vidal, M. J. Zeiger, G. Dresselhaus, M. S. Dresselhaus, and E. P. Ippen, Appl. Phys. Lett. **57**, 1004 (1990).

[4]J. M. Chwalek, C. Uher, J. F. Withaker, and G. A. Mourou, Appl. Phys. Lett. **58**, 980 (1991).

[5]T. Pfeifer, R. Scholz, and H. Kurz, Phys. Rev. Lett. **69**, 3248 (1992).

[6]Y. X. Yan and K. A. Nelson, J. Chem. Phys. **87**, 6240 (1987); Y. X. Yan and K. A. Nelson, **87**, 6257 (1987).

[7]T. Pfeifer, T. Dekorsy, W. Kütt, and H. Kurz, Appl. Phys. A **55**, 482 (1992); W. Kütt, W. Albrecht, and H. Kurz, IEEE J. Quantum Electron **28**, 2434 (1992).

[8]R. Scholz and A. Stahl, Phys. Status Solidi B **168**, 123 (1991).

[9]T. K. Cheng, J. Vidal, H. J. Zeiger, G. Dresselhaus, M. S. Dresselhaus, and E. P. Ippen, Appl. Phys. Lett. **59**, 1923 (1991); H. J. Zeiger, J. Vidal, T. K. Cheng, E. P. Ippen, G. Dresselhaus, and M. S. Dresselhaus, Phys. Rev. B **45**, 768 (1992).

[10]B. S. Wherrett, A. L. Smirl, and T. F. Boggess, IEEE J. Quantum Electron. **19**, 690 (1983).

[11]W. Huhn and A. Stahl, Phys. Status Solidi B **124**, 167 (1984); A. Stahl and I. Balslev, *Electrodynamics of the Semiconductor Band Edge,* Springer Tracts in Modern Physics Vol. 110 (Springer-Verlag, Berlin, 1987); J. Schlösser and A. Stahl, Phys. Status Solidi B **153**, 773 (1989).

[12]H. Haug, in *Optical Nonlinearities and Instabilities in Semiconductors,* edited by H. Haug (Academic, London, 1988), p. 53.

[13]M. Hartmann and W. Schäfer, Phys. Status Solidi B **173**, 165 (1992).

[14]R. Scholz and A. Stahl, Phys. Status Solidi B **173**, 199 (1992).

[15]W. Z. Lin, R. W. Schoenlein, J. G. Fujimoto, and E. P. Ippen, IEEE J. Quantum Electron. **24**, 267 (1992).

[16]R. Scholz, Ph.D. thesis, Kurzzeit-Dynamik von Randfeldern und kohärente Phononen in III-V-Materialien, edited by B. U. Felderhoff, P. Grosse, A. Stahl, and D. Vollhardt, ABPKM Vol. 1 (Verlag der Augustinus-Buchhandluug, Aachen, 1992).

[17]R. Zimmermann, J. Lumin. **53**, 187 (1992); T. Kuhn and F. Rossi, Phys. Rev. B **46**, 7496 (1992).

[18]R. Scholz, A. Stahl, X. Q. Zhou, K. Leo, and H. Kurz, IEEE J. Quantum Electron. **28**, 2473 (1992).

[19]M.L. Cohen and J. R. Chelikowsky, *Electronic Structure and Optical Properties of Solids,* Springer Series in Solid-State Sciences Vol. 75 (Springer, Berlin, 1988).

[20]L. Viña, S. Logothetidis, and M. Cardona, Phys. Rev. B **30**, 1979 (1984).

[21]P. C. Becker, H. L. Fragnito, C. H. Brito-Cruz, J. Shah, R. L. Fork, J. E. Cunningham, J. E. Henry, and C. V. Shank, Phys. Rev. Lett. **61**, 1647 (1988).

[22]V. Heine, *Group Theory in Quantum Mechanics, International Series and Monographs on Pure and Applied Mathematics,* edited by I. N. Sneddon and S. Ulam (Pergamon, London, 1960), Vol. 9; G. L. Bir and G. E. Pikus, *Symmetry and Strain-induced Effects in Semiconductors* (Wiley, New York, 1974).

[23]G. F. Koster, J. O. Dimmock, R. G. Wheeler, and H. Statz, *Properties of the Thirty-Two Point Groups* (MIT Press, Cambridge, MA, 1963).

[24]M. Cardona, in *Light Scattering in Solids II,* edited by M. Cardona and G. Güntherodt, Topics in Applied Physics Vol. 50 (Springer, Berlin, 1982), p. 19.

[25]J. F. Nye, *Physical Properties of Crystals* (Oxford University Press, London, 1957); Y. R. Shen, *The Principles of Nonlinear Optics* (Wiley, New York, 1984).

[26]E. O. Kane, J. Phys. Chem. Solids **1**, 249 (1957).

[27]B. P. Zakharchenya, D. N. Mirlin, V. I. Preel, and I. I. Reshina, Usp. Fiz. Nauk **136**, 459 (1982) [Sov. Phys. Usp. **25**, 143 (1982)]; G. Fasol, W. Hackenberg, H. P. Hughes, K. Ploog, E. Bauser, and H. Kano, Phys. Rev. B **41**, 1461 (1990).